Indian Geotech J (October 2022) 52(5):1226–1243
https://doi.org/10.1007/s40098-022-00616-0

ORIGINAL PAPER

Internal Instability and Fluidisation of Subgrade Soil under Cyclic Loading

Buddhima Indraratna[1] · Mandeep Singh[2] · Thanh Trung Nguyen[1] · Cholachat Rujikiatkamjorn[1] · Rakesh Sai Malisetty[1] · Joseph Arivalagan[3] · Lakshmi Nair[3]

Received: 3 February 2022 / Accepted: 22 March 2022 / Published online: 23 June 2022

Abstract Rapid globalisation and the rise in population have substantially increased the demand for rail infrastructure which have been critical in transporting passengers and freight across landmasses for over a century. The surge in demand often leads to the construction of railway lines along with unfavourable soil conditions which result in different forms of substructure challenges such as uneven track deformations, ballast degradation, and subgrade mud pumping. A widespread site investigation along the eastern coast of New South Wales, Australia, indicated the prevalence of mud holes or bog holes along the tracks. The field studies suggest that low-to-medium plasticity soils are highly susceptible to mud pump when subjected to heavy axle loads under impeding drainage conditions. Subsequent laboratory investigations conducted on the remoulded soil samples collected from the sites indicated the sharp rise in cyclic axial strains and excess pore pressures along with the internal redistribution of moisture content as the governing mechanism for mud pumping. Numerical simulations performed using discrete element method coupled with computational fluid dynamics show that at a high hydraulic gradient, there is a substantial loss of soil contact network which leads to the upward migration of soil particles. The role of plastic fines and the inclusion of geosynthetic layer between the ballast and subgrade are also discussed in this paper. It was observed that the addition of 10% of cohesive fines increased the resistance of subgrade soils to mud pumping. On the other hand, geosynthetic inclusions not only assist in dissipating high cyclic excess pore pressures but also inhibit the upward migration of fine particles.

Keywords Subgrade instability · Mud pumping · Cyclic triaxial test · CFD-DEM · Geosynthetics

✉ Buddhima Indraratna
buddhima.indraratna@uts.edu.au

[1] Transport Research Centre, University of Technology Sydney, Ultimo, NSW 2007, Australia

[2] School of Civil and Environmental Engineering, University of Technology Sydney Tech Lab, , Botany, NSW 2019, Australia

[3] Transport Research Centre, School of Civil and Environmental Engineering, University of Technology Sydney, Ultimo, NSW 2007, Australia

Introduction

Rail transportation is a vital component of a national economy as it is the most prominent transport mode carrying both freight and passengers across places [1, 2]. The burgeoning population and intensified trade necessitate the increase in the speed of passenger trains and the weight norms of freight trains. This surge in demand for railways has led to significant studies being conducted in rail track geodynamics. Several factors need to be considered while designing a railway track, viz. train speed, loading intensity, stiffness of the subsoil, track routes, affordability, maintenance costs, and environmental impact [3].

A typical ballasted rail track comprises of two sections, namely the superstructure and substructure. The superstructure includes rails, sleepers, and fastenings, whereas the substructure involves the most critical foundation layers of the railway track. It consists of the ballast, subballast, and subgrade layers. Some of the commonly reported deformations associated with the railway track include differential track settlement [2], ballast fouling [4–6], track buckling [7], and subgrade failures [8–14]. The

major subgrade problems include progressive shear failure [8, 10], excessive plastic deformation (ballast pockets) [13], and mud pumping [9, 15]. These conditions are responsible for increased track maintenance costs which can outweigh the economic benefits of carrying cargo on rails. Therefore, it is imperative to study the behaviour and deformation characteristics of subgrade under dynamic loads.

Of all the challenges mentioned above, track fouling due to mud pumping is a significant issue faced by railways worldwide [15–19]. Mud pumping is often manifested as a dry soil deposit or wet mud slurry on the track surface, or sometimes as an interlayer created between ballast/subgrade layers [12, 20–22]. The prominent factors that lead to the pumping of subgrade fines include high excess pore water pressure, the presence of finer subgrade fraction, and cyclic loading from the passage of trains [17, 19, 23]. The complex combination of these factors results in subgrade mud pumping. In addition to these factors, conditions such as improper sleeper ballast contact or tie-ballast contact creating suction [24], freeze–thaw cycles in cold regions changing structure, moisture content, and strength of soil, may cause subgrade fluidisation [17, 18, 25] which results in the mud slurry being ejected onto the surface. Apart from the internal conditions, some external agents such as non-subgrade fines can induce mud pumping. These include but are not limited to fines from ballast breakage, sleeper wear, coal spillage, wind, and waterborne dust, which reduce the drainage capability and adversely affect the ballast's mechanical functions [2, 26, 27]. It has been quantified that a majority (76%) of fouling material in ballast is contributed by ballast breakage, followed by migration of fines from sub-ballast and subgrade (16%) and a small amount (7%) is infiltrated from the surface [28]. Fouled ballast with a hydraulic conductivity less than 1×10^{-4} m/s is deemed to be unacceptable for railway tracks [2]. Any lower permeability would in turn lead to ballast acting as a drainage barrier increasing the susceptibility of mud pumping. Figure 1 shows the various sources of ballast fouling, which strongly indicate a significant contribution (i.e., 58%) from the subgrade and sub-ballast layers.

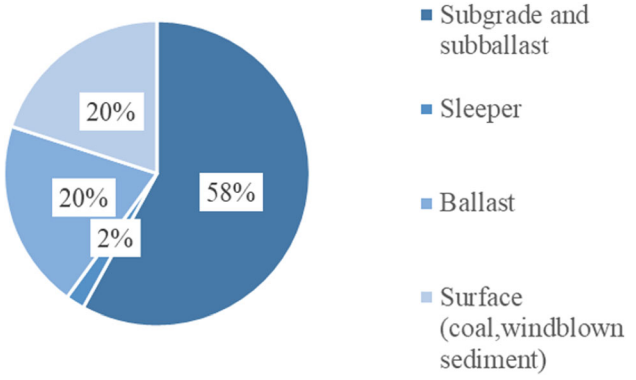

Fig. 1 Comparison of different sources of ballast fouling (modified after Indraratna et al. [27])

In low-lying coastal areas, where the subgrade soils are soft and saturated, the pumping of subgrade fines due to soil fluidisation is a major concern [15]. The soils with a high fine fraction (less than 75 μm) and filter ratio ($D_{15\text{-coarse}}/D_{85\text{fine}}$) greater than four can become internally unstable when subjected to high pore pressure [29]. During the generation of excess pore pressure under repeated loads and poor drainage conditions, clay particles having a high specific surface area adsorb water and forms slurry. This process of subgrade fluidisation is dependent on the loading amplitude and frequency, and it is necessary to investigate the behaviour of subgrade soil under these conditions with poor drainage. Although in recent times, experimental investigations to study the phenomenon of slurry formation and migration under cyclic loading have been reported [29–31], there are limited insights into the response of a soil element. The localised response of the soil specimen to cyclic loading associated with the degradation in shear stiffness requires an in-depth investigation.

This paper aims to explore the aspect of subgrade mud pumping by carrying out extensive field investigations along the south-eastern coast of New South Wales Australia. The role of ballast breakage on fouling was also studied. Further, attempts were made to clarify the mechanisms of mud pumping by conducting undrained cyclic triaxial tests on remoulded subgrade soils subjected to varying cyclic stress ratio (CSR), loading frequency (f), relative density, plastic fines, etc. The results indicate that the complex interaction of these factors triggers the excessive deformation and high cyclic excess pore pressures, leading to the internal redistribution of water content which at high hydraulic gradient leads to subgrade fluidisation. The redistribution of the soil particles and moisture contents at high hydraulic gradients was examined through discrete element method (DEM) simulations coupled with complex computational fluid dynamics (CFD). Towards the end of the paper, the authors also report the role of geosynthetic inclusions in preventing subgrade fluidisation.

The current mitigation techniques to prevent the occurrence of mud pumping range from subgrade soil stabilisation using cementitious materials [32]; geosynthetic inclusions [15, 30]; and prefabricated vertical drains [33–36]. Recent studies indicate that subgrade soil vulnerable to fluidisation has a liquid limit in the range of 20 to 50 and plasticity index < 30 [9, 17]. Hence, there is a need to examine the role of adding cohesive fines, thereby increasing the soil plasticity and investigating the cyclic response of the subgrade soils. Further, this paper also ventures into exploring the potential of geosynthetic

inclusions by carrying out tests on modified filtration apparatus.

Site Reconnaissance and Soil Characteristics

Considerable effort has gone into investigating mud pumping under railways in recent years; however, most studies mainly focused on laboratory tests due to the lack of resources [29, 30, 37]. Therefore, a thorough field investigation followed by extensive laboratory testing was carried out along the South Coast Illawarra railway line in New South Wales (Australia) with the support of Sydney Trains. This investigation concentrated on sites commonly known as bog holes (i.e., slurry track), where the track fouling condition was severe.

Brief Description of Site Investigation

The Illawarra line connects Sydney to its Southeast regions, i.e., Nowra (Fig. 2a) is a shared rail network between passenger and freight transport. Train speeds vary from 40 to 110 km/h depending on the curvature of the track, the axle load, and the length of trains. The freight service mainly carries coal (i.e., about half of the total volume of freight) and other grain materials with the largest axle load of 25 tonnes. The site investigation went through twenty different locations from more than 300 bog holes reported along coastal regions in NSW, and 100 places on the South Coast (SC) line [9]. The current study mainly focuses on the segment from Waterfall to Nowra (Sydney's outskirts) due to the ease of access. Figure 2b shows a typical location of a mud hole (white fines) that caused severe track deterioration. In wet weather conditions, these fines become slurry and function as a lubricant reducing ballast friction.

Three major tasks were carried out at each mud pumping location: (i) an assessment of site conditions and track degradation, (ii) material sampling, and (iii) laboratory testing. Task (i) included evaluating drainage and track conditions such as side ditches, water ponding, the size of mud pumping zone, visual observations of track deterioration, and ballast fouling. Task (ii) was to collect subgrade soil, mud, and fouled ballast samples for laboratory tests (Fig. 2c). Apart from the fundamental soil characterisation tests such as Atterberg limits, particle size distribution (PSD), hydraulic conductivity, a series of undrained cyclic triaxial tests were also carried out to understand behaviour of subgrade foundation under rail loads. The cyclic triaxial tests will be discussed in the later sections.

Field Observations

Most of the investigated sites had poor drainage conditions which were found to be the major contributor to undrained subgrade behaviour. The common issue that came across different mud pumping tracks was improper and insufficient side ditches which did not provide sufficient drainage capability for the track foundation. The spillage of coal and construction materials was also a factor causing track fouling and reduced drainage capacity. In some locations where the track runs through the escarpment, the transverse gradient from higher to lower side washed soil particles and debris into the tracks, leading to the accumulation of fines and the formation of mud. In the low-lying sites, i.e., from Wollongong to Nowra where the elevation of the track from the sea level is about 30 to 50 m, saturated subgrade under heavy rail loads and poor drainage fluidised and intruded into the ballast.

Figure 3 shows the particle size distribution (PSD) of fouled ballast at various mud pumping locations. The results show that a considerable mass of fine particles (< 75 μm) especially clay particles from the subgrade in the fouling materials, causes the PSD to deviate from the standard ballast gradation. The laboratory tests (Table 1) indicate that mud fines had low to medium plasticity (PI ≤ 22). The clay content exceeded 40% at some locations; however, the mineral analysis (X-Ray diffraction) shows that the majority of clay minerals were kaolinite which implies the soils were less plastic and cohesive compared to other clay minerals.

Effect of Fouling on Ballast Permeability

Fouling of ballast can be quantified using a unique void contamination index which considers the change in void ratio due to fouling as well as the specific gravity of different fouled materials as shown below [5].

$$\mathrm{VCI} = \frac{1 + e_f}{e_b} \times \frac{G_{sb}}{G_{sf}} \times \frac{M_f}{M_b} \times 100 \quad (1)$$

where e_f and e_b are the void ratios, G_{sb} and G_{sf} are the specific gravities, and M_f and M_b are the masses of fouling material and clean ballast respectively. A VCI of 50% indicates that half of the voids are filled with fouling material.

Various studies [5, 38] have shown that fouling of ballast not only impacts the load bearing capacity of the track due to its reduced shear strength but also affects the track condition by creating localised mud pockets, subsequently leading to the generation of excess pore water pressures in

Fig. 2 Site investigation on mud pumping rail tracks: **a** map of the South Coast Illawarra (SC) rail line with bog hole locations, **b** severe fouling of rail track due to mud pumping, and **c** excavation and sampling

the subgrade layers. However, different fouling materials such as coal fines and clay are found to affect the permeability of ballast to different extents, owing to the difference in their permeability. Experimental tests conducted on fouled ballast using large-scale permeability apparatus indicated that the overall hydraulic conductivity was reduced with an increase in VCI for all the fouling materials as shown in Fig. 4. The hydraulic conductivity of ballast was initially reduced by 200 times for a 5% VCI fouled with coal fines respectively, while the effect plateaued after 75% with the permeability remaining in the acceptable limits for acceptable track operations. In contrast, the reduction in hydraulic conductivity was relatively low at VCI = 10% of clay fouling (Kaolin clay with a plasticity index of 26% and liquid limit of 51.6% was used as fouling material), but a steady reduction of permeability is observed with an increase in VCI for clay-fouled ballast. This almost reached the permeability of plastic fines at a VCI of 90%, indicating that the ballast loses its ability to free drain and further acts as a drainage impediment,

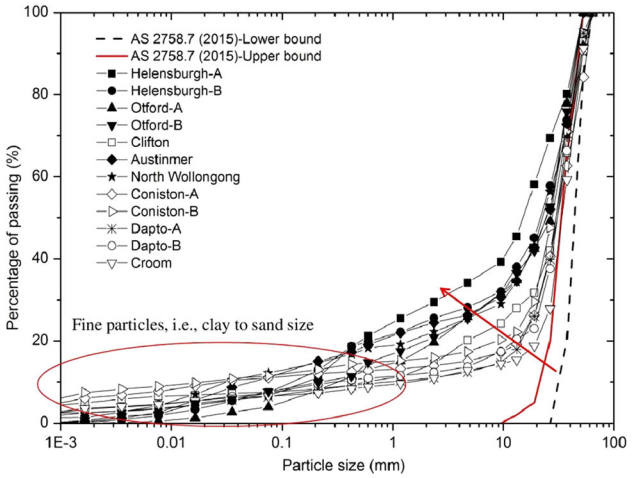

Fig. 3 Particle size distribution (PSD) of fouled ballast due to mud pumping

leading to the generation of excess pore water pressures in soft saturated subgrades causing pumping.

Cyclic Behaviour of Subgrade Prone to Mud Pumping

Basic Soil Properties

Soil samples were collected from a pumping prone site near Wollongong City to investigate the cyclic behaviour of the subgrade soil. Preliminary geotechnical tests indicated the soil as low plastic clay, CL having a liquid limit of 26, and a plasticity index of about 11 [39]. This is consistent with other findings where mud pumping incidents were identified mostly for fine-grained soils having a low to moderate plasticity index (i.e., PI < 26) [17, 29, 30, 40–42].

The samples of natural subgrade soil were reconstituted using nonlinear under-compaction method [29] to produce test specimens of different compacted dry densities (ρ_d), i.e., ρ_d = 1600, 1680, and 1790 kg/m^3, and then were tested to investigate the undrained cyclic response.

Undrained Cyclic Triaxial Testing Programme

A series of stress-controlled undrained cyclic triaxial tests at low confining stress was performed on the reconstituted specimens. An effective confining pressure of $\sigma_c^{'}$ = 15 kPa was employed as it simulated the shallow subgrade region which is vulnerable to pumping. The cyclic response of the subgrade samples was examined using the GDS ELDYN dynamic triaxial system which consisted of an axially stiff loading frame with an electro-mechanical actuator.

The cyclic stress ratio (CSR) is defined as the ratio of the applied dynamic stress (σ_d) to twice the effective confining pressure ($\sigma_c^{'}$), as follows:

$$\mathrm{CSR} = \frac{\sigma_d}{2\sigma_c^{'}} \tag{2}$$

A back pressure of 400 kPa was applied over 24 h to ensure that specimens achieved a Skempton's B

Table 1 Properties of mud fines collected at the surface zone of fouled tracks

No	Location	Liquid limit LL	Plastic limit PL	Plasticity index PI	Specific gravity G_s	Hydraulic conductivity (m/s)	Fines content ($\leq$ 0.075 mm) (%)	Clay content ($\leq$ 0.002 mm) (%)
1	Helensburgh A	30	23	7	2.56	4.3×10^{-6}	26.3	7.6
2	Helensburgh B	23	18	5	2.51	9.1×10^{-6}	28.9	1.0
3	Otford A	21	16	5	2.51	1.1×10^{-5}	19.8	1.1
4	Otford B	23	17	6	2.50	7.8×10^{-6}	36.7	2.9
5	Clifton	38	18	20	2.69	6.1×10^{-7}	51.7	33.8
6	Austinmer	24	19	5	2.53	6.5×10^{-6}	45.3	1.8
7	North Wollongong	27	20	7	2.43	2.8×10^{-6}	54.5	6.2
8	Coniston A	44	22	22	2.65	1.7×10^{-7}	78.9	43.2
9	Coniston B	40	20	20	2.66	2.3×10^{-7}	72.2	46.5
10	Dapto A	39	22	17	2.62	7.2×10^{-7}	58.4	22.5
11	Dapto B	38	20	18	2.67	6.8×10^{-7}	58.6	27.0
12	Croom	37	19	19	2.69	6.6×10^{-7}	59.5	32.4

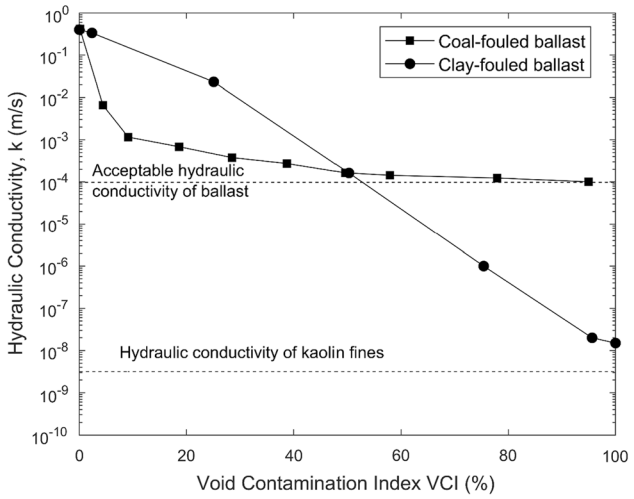

Fig. 4 Effect of coal and clay fouling on the hydraulic conductivity of fouled ballast (modified after Tennakoon et al. [5])

value > 0.95. Then, the specimens were anisotropically consolidated at a k_0 = 0.6 and an effective confining stress of $\sigma_c^{'}$ = 15 kPa. A sinusoidal waveform of cyclic load was then applied, and the excess cyclic pore pressure was measured using a pore pressure transducer located at the bottom of the test specimen. The tests were concluded when the permanent axial strains reached either 5% or when the number of cycles reached 50,000. Appropriate membrane correction for the analysis was applied according to [43]. Figure 5 shows the representation of the specimen fluidising in the GDS ELDYN equipment and forming a liquid-like state at the top when subjected to a high CSR.

Cyclic Response of Tested Specimens

The cyclic stress ratio plays a crucial role on the behaviour of specimen. Specifically, there exists a critical cyclic stress ratio (CSR_c), where the excess pore pressure (EPP) and axial strains begin to increase rapidly with a substantial drop in the deviatoric stress q, indicating the inception of fluidisation. The value of the CSR_c is dependent on the initial dry density of the soil specimen and the loading frequency. For example, as can be seen from Fig. 6, the CSR_c for a specimen compacted at a dry density of 1680 kg/m^3 and subjected to a loading frequency of 1.0 Hz is somewhere between 0.3 and 0.4. Indraratna et al. [29] reported the similar effect of initial dry density and loading frequency on the critical cyclic stress ratio. In addition to the rapid increment in the cyclic axial strains and excess pore pressure ratio, the fluidised specimens experienced an early softening type behaviour [14, 31]. As shown in Fig. 7, for the unstable specimens (wherein the CSR ≥ CSR_c), there was a reduction in the applied peak cyclic stress due to early softening. As the top of the specimen fluidised, it was unable to withstand the high magnitude of the applied cyclic stress.

Stiffness Degradation Index, δ

As soils experience large strains, there is a considerable reduction in the soil stiffness. While some past studies [44, 45] have calculated the stiffness degradation by assuming a constant level of stress, it may not be applicable for the fluidised specimens as they experience early softening (as indicated in Fig. 7). Therefore, Singh et al. [14]

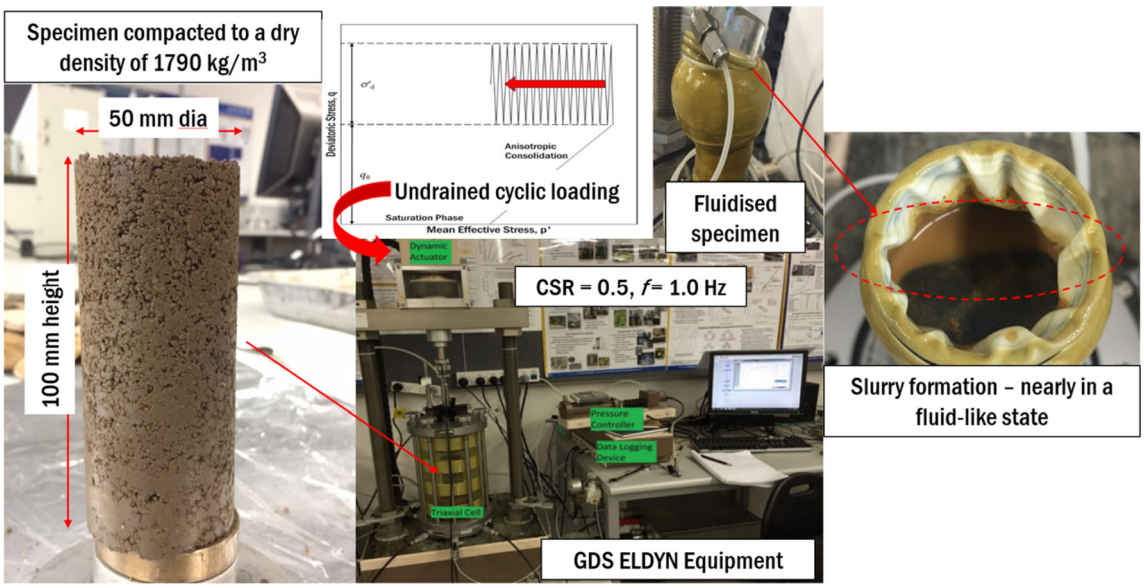

Fig. 5 Undrained cyclic triaxial test on a compacted specimen (ρ_d = 1790 kg/m^3) fluidising at a CSR = 0.5, f = 1.0 Hz

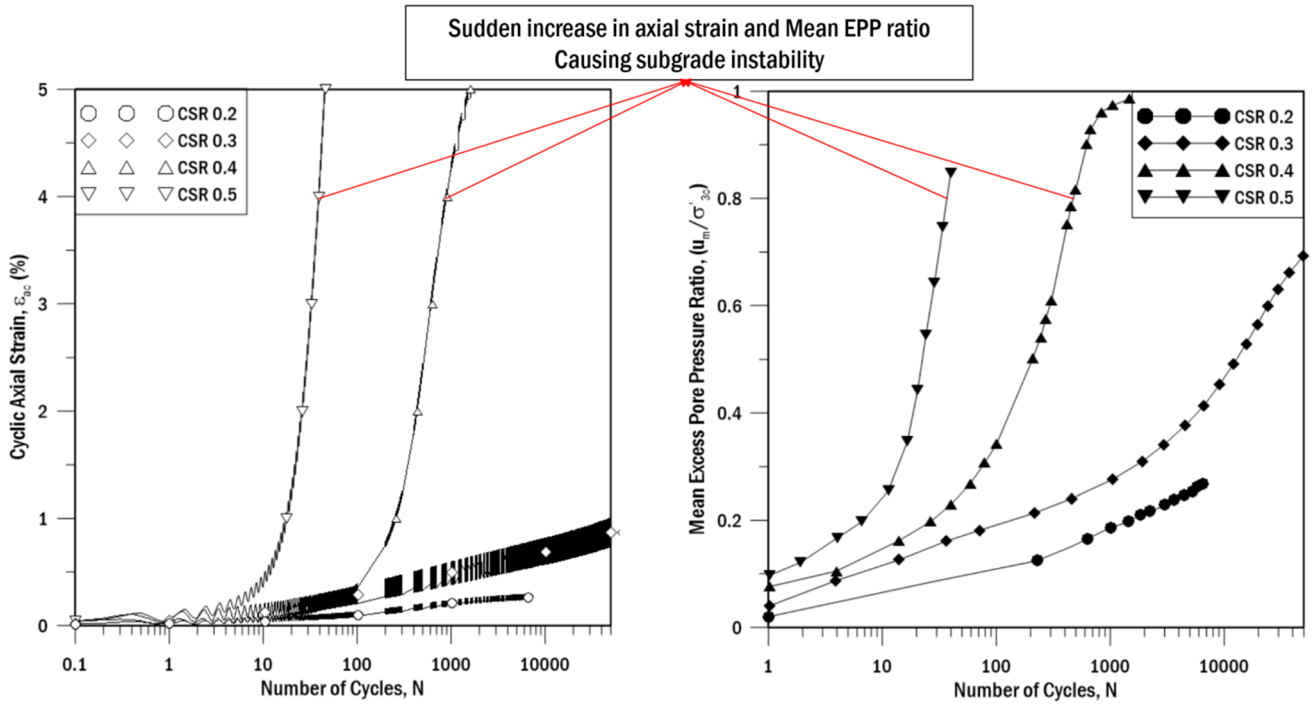

Fig. 6 Variation of the cyclic axial strain and mean excess pore pressure ratio for specimens compacted at ρ_d = 1680 kg/m^3 at a loading frequency of 1.0 Hz

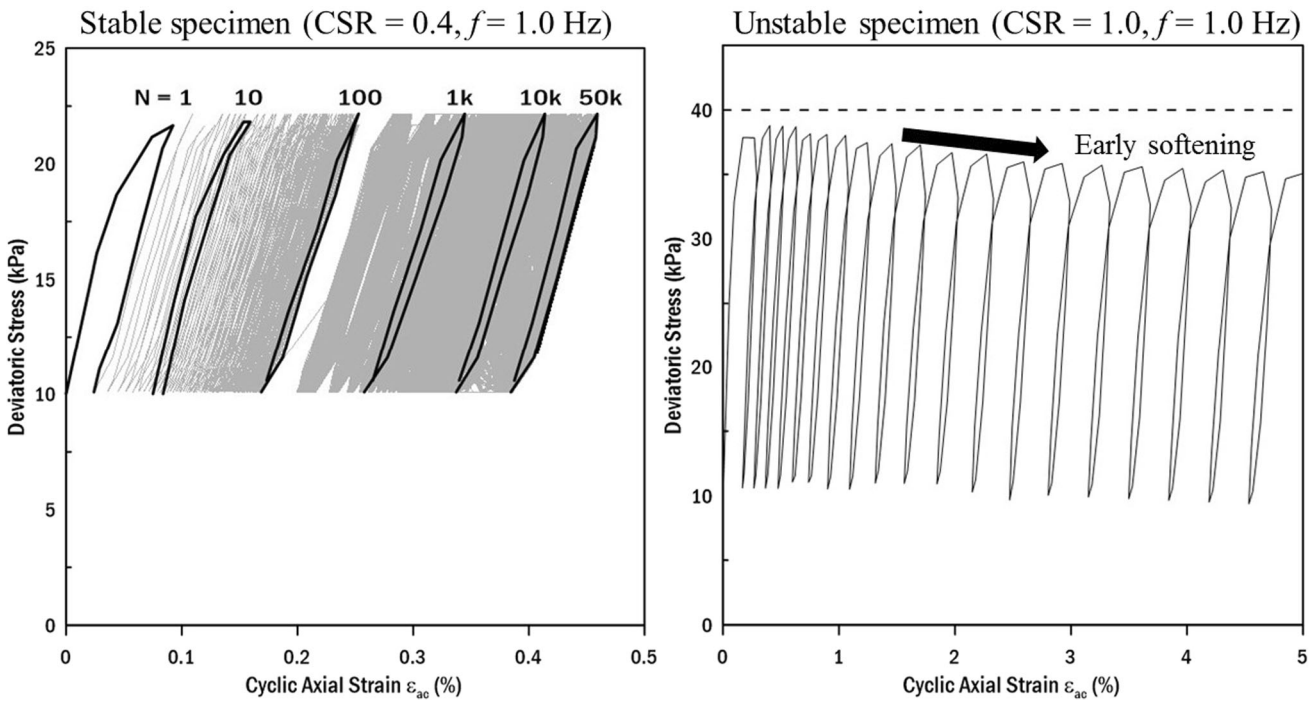

Fig. 7 Stress–strain response for the stable (CSR < CSR$_c$) and unstable specimen (CSR ≥ CSR$_c$) for specimen compacted at ρ_d = 1790 kg/m^3 (Singh et al. [14])

adopt the use of axial dynamic modulus of each loading–unloading cycle to evaluate the stiffness degradation index, δ.

The axial dynamic stiffness was defined as the ratio of the difference of maximum and minimum deviatoric stress

to the difference of the maximum and minimum axial strain at N number of cycles [14]:

$$E_{d,N}=\left[\frac{\sigma_{d,max}-\sigma_{d,min}}{\varepsilon_{d,max}-\varepsilon_{d,min}}\right]_N \quad (3)$$

The stiffness degradation index, δ, was computed by calculating the ratio of the axial dynamic stiffness of a given cycle to that of the first cycle:

$$\delta=\frac{E_{d,N}}{E_{d,1}} \quad (4)$$

In order to estimate the critical number of cycles, the degradation index plots are graphed along with the mean excess pore pressure ratio plots. The point of intersection of the two curves was defined as the threshold number of cycles, N_{thr}, assumed to be the onset of fluidisation [14]. As can be seen from Fig. 8, there exists a quasi-linear relationship between $\varepsilon_{ar,thr}$ and $\log(N_{thr})$ at a given cyclic stress ratio; however, the applicability for a wide range of soils is yet to be investigated [14].

Localised Response of Subgrade Specimens

Upward Migration of Fines for the Fluidised Specimens

As reported in the above sections, the specimens subjected to higher CSR (> CSR_c) fluidised and it was noted the top portion of the specimen turned to a fluid-like state (Fig. 5). After the test was concluded, the specimen was carefully removed from the triaxial chamber, and the gradation was analysed. The top and middle one-third regions were tested in the Malvern particle size analyser (Mastersizer). From Fig. 9, it is evident that there was a significant amount of fines (< 75 μm) that migrated towards the top regions of the test specimen (≈ 36%) as opposed to that of the middle region (≈ 24%). This implies that during the application of cyclic loading, there is an upward movement of finer fraction transported by the moisture content, thereby facilitating the formation of a slurry or suspension in near the top portion of the specimen [29].

Change in Liquidity Index

Indraratna et al. [31] measured the water contents at 4 different locations from the bottom to the top of specimens after the cyclic test and reported a considerable redistribution of the moisture content along with the sample height. It was characterised by evaluating the liquidity index (LI) that captures the water content relative to the plastic and liquid limits. Clearly, the liquidity index of fluidised specimens varied widely from top to bottom (0.5–0.9) (Fig. 10). While the LI of the top part is nearly 1.0 representing a fluid-like state, it is about 0.5 towards the bottom. As the specimens were fully saturated during the test, the redistribution of water content in specimens was caused by cyclic loading, implying that the variation in void ratio and dry density would occur along the vertical axis (height) of specimens after the cyclic test [31].

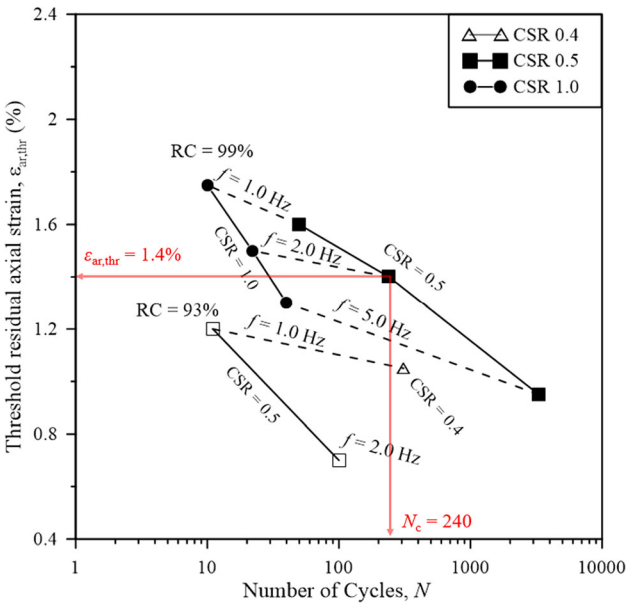

Fig. 8 Variation of the threshold residual strain at different cyclic loading conditions (modified after Singh et al. [14])

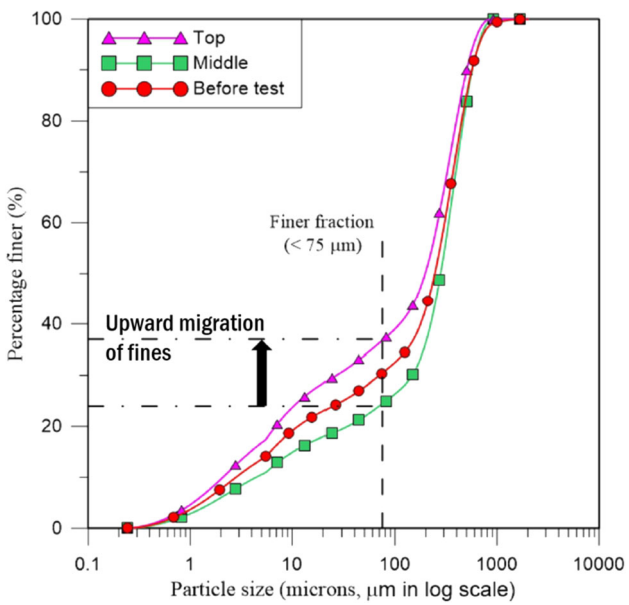

Fig. 9 Migration of finer fraction for the fluidised specimens (modified after Indraratna et al. [46])

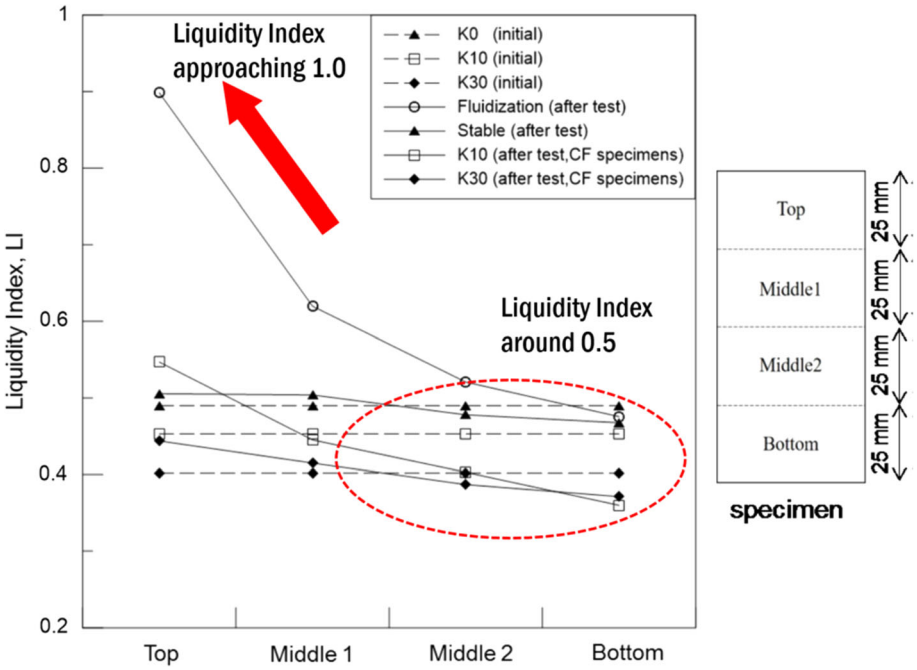

Fig. 10 Variation of the liquidity index along the specimen height (modified after Indraratna et al. [31])

Particulate Behaviour During Fluidisation

Introduction to CFD-DEM Technique

As seen from the previous section, the localised behaviour of a fluidised soil specimen is one of the most challenging aspects that hamper conventional methods such as the finite element method (FEM) and analytical method from accurate prediction. The migration of pore water accompanied by soil particles over different soil layers is an intrinsic phenomenon during soil fluidisation, and it requires a more sophisticated approach to capture the soil and fluid interactions. In this section, discrete element method (DEM) coupled with the computational fluid dynamics (CFD) was used to address soil fluidisation under an increasing hydraulic gradient due to an upward seepage flow.

Theoretical Background

The motion of soil particles considering the effect of fluid is governed by the following equations based on the second Newton's law:

$$m_i \frac{d\boldsymbol{U}_{pi}}{dt} = \sum_{j=1}^{n_i^c} \boldsymbol{F}_{cij} + \boldsymbol{F}_{gi} + \boldsymbol{F}_{fi} \tag{5}$$

$$I_i \frac{\omega_{pi}}{dt} = \sum_{j=1}^{n_i^c} \left(M_{c,ij} + M_{r,ij}\right) \tag{6}$$

where $\boldsymbol{U}_{pi}$ and ω_{pi} are the translational and angular velocities of particle i, respectively; m_i is the mass of particle; $\boldsymbol{F}_{c,ij}$, $\boldsymbol{F}_{g,i}$, and $\boldsymbol{M}_{c,ij}$ are the contact, gravitational forces, and torque acting on particle i by particle j (or walls) while n_i^c denotes the number of total contacts of particle i. $\boldsymbol{M}_{r,ij}$ is the rolling friction torque. The nonlinear Hertz-Mindlin contact model and the directional constant torque model to capture rolling friction are employed; the details of these applications can be found in previous studies [47]. In the current study, the density of soil particles is 2650 kg/m^3; Poisson ratio is 0.3; Young's modulus is 6.8×10^{-7} Pa; and coefficients of sliding and rolling friction are 0.5 and 0.1, respectively.

The fluid behaviour is captured based on Navier–Stokes (NS) equations as follows:

$$\frac{\partial n_f}{\partial t} + \nabla.\left(n_f \boldsymbol{U}_f\right) = 0 \tag{7}$$

$$\frac{\partial\left(\rho_f n_f \boldsymbol{U}_f\right)}{\partial t} + \nabla.\left(\rho_f n_f \boldsymbol{U}_f \boldsymbol{U}_f\right) = -n_f \nabla p + \nabla.\left(n_f \boldsymbol{\tau}_f\right) + \rho_f n_f \boldsymbol{g} - \boldsymbol{f}_p \tag{8}$$

where ρ_f, τ_f, U_f, and p are the density, viscous stress, velocity, and pressure of fluid, respectively; n is the porosity while g is the gravitational acceleration vector; f_p is the mean volumetric particle–fluid interaction force which is added into the conventional NS's momentum equation to represent the effect of solid particles on the fluid phase. Details of computing f_p considering subgrade soil properties can be found in recent studies [48].

Behaviour of solid and fluid phases is computed individually using DEM based on LIGGGHTS and OpenFOAM; however, the parameters are exchanged with each other in every pre-defined number of time steps. The total

hydraulic force acting on particles primarily includes the pressure gradient force, the viscous force, and the drag force. The method to compute and combine these forces can be found elsewhere [47, 48].

Soil Selection and Model Set-up

Previous studies [17] indicated that low plasticity soil is highly susceptible to fluidisation, the current model hence selected a cohesionless soil which was subjected to the experimental study of hydraulic failure, i.e., piping and fluidisation [49]. Particle size distribution (PSD) of this soil is shown where experimental and numerical (DEM) data agree with each other very well. The soil is formed in a cubical element using periodic boundary to eliminate the effect of soil-wall interactions. Figure 11 shows this soil is subjected to an upward fluid flow which is modelled by CFD. Porosity of the soil was 0.32 with respect to the experimental value, while the hydraulic gradient is increased gradually until the complete fluidisation of soil. This increase in the hydraulic gradient aims to simulate the localised excess pore pressure over the depth of subgrade soil that can be generated by the passage of trains. The variation in hydraulic conductivity, particle migration, and soil deformation were computed over time.

Analysis of the Numerical Simulations

Figure 12 shows the predicted hydraulic conductivity of the soil based on the current numerical method in comparison with experimental data. The results show relatively good agreement between the numerical and experimental curves. Increasing hydraulic gradient results in a linear increase in the discharge velocity of the seepage flow; however, as the hydraulic gradient reaches a critical value, i.e., 1.7, the hydraulic conductivity increases rapidly. This is indicated by the turning point in the flow curve as seen in Fig. 12. The major reason for this substantial increase is because increasing hydraulic gradient enhances the hydraulic forces acting on soil particles, making the soil particle displace upward accompanied with increase in porosity of the soil specimen.

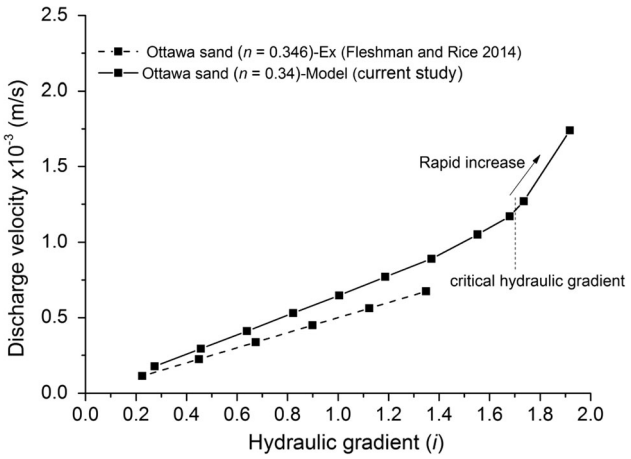

Fig. 12 Hydraulic behaviour of soil under increasing hydraulic gradient

Deformation of the soil specimen under increasing hydraulic gradient is shown in Fig. 13a. It is apparent that there is a significant heave that is formed due to the

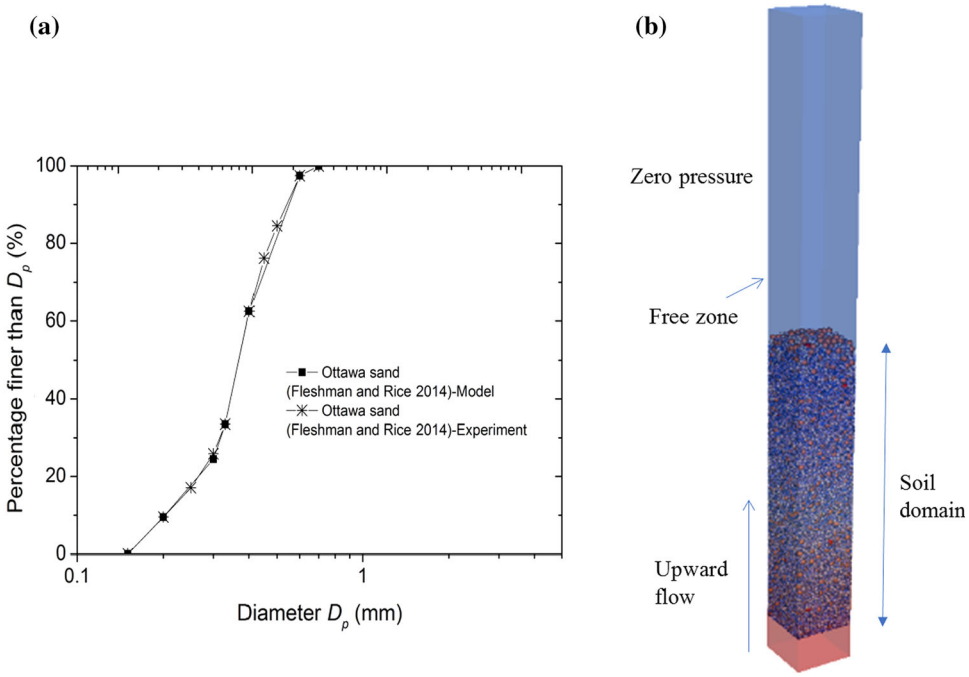

Fig. 11 **a** Particle size distribution of the selected soil for modelling and **b** soil element in DEM coupled with upward fluid flow

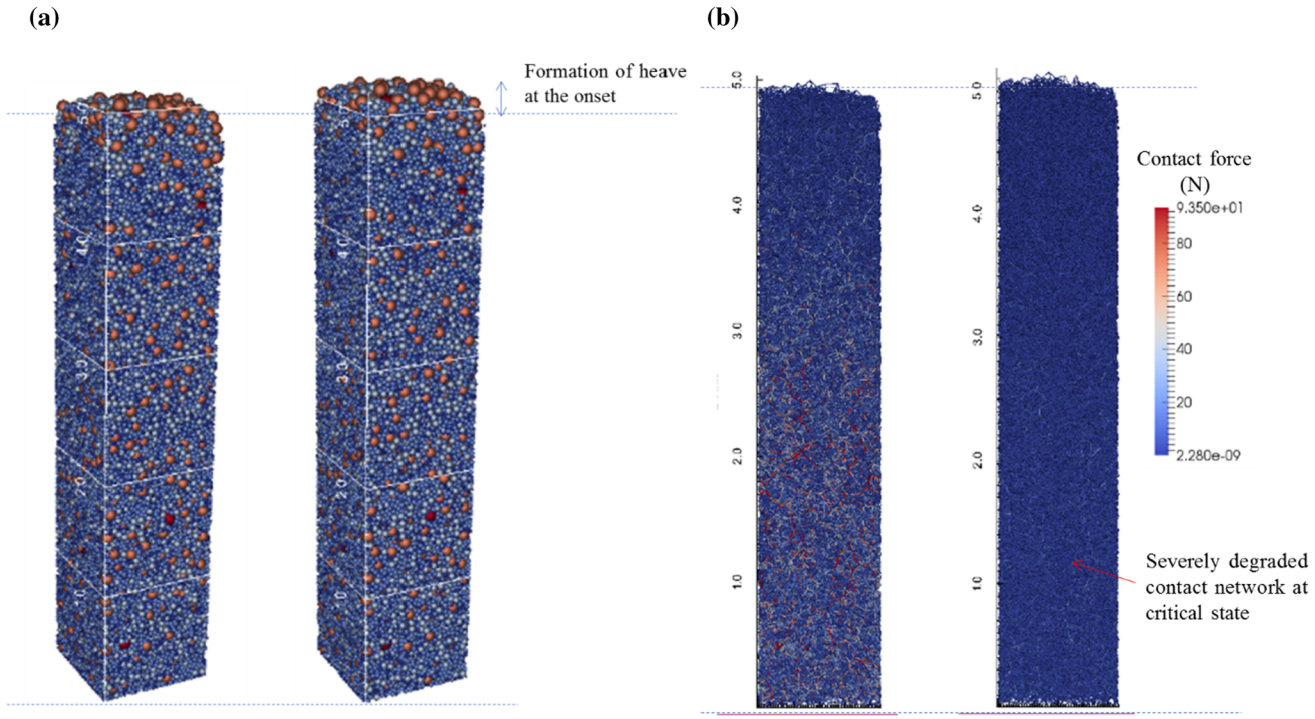

Fig. 13 Soil degradation at critical state: **a** heave formation, and **b** losing contact network of soil particles

increase in hydraulic gradient. Specifically, the current simulation estimated a vertical displacement of the soil surface of about 6.5% of the total height of the specimen at the onset of the critical state. Further, an increase in hydraulic gradient leads to a swift displacement of the soil surface and upward migration of soil particles, i.e., all particles are floating under zero-effective stress, thus causing soil fluidization. Figure 13b shows that the contact network of soil particles is degraded at the critical state. It is apparent that the strength of particle contacts decreases substantially to near zero at many places. It also means that the soil has lost a majority of its stiffness and particles are not restrained at this stage; thus, they are free to migrate if a larger hydraulic gradient is applied.

Remediation Measures for Subgrade Mud Pumping

Addition of Plastic Fines into the Soil Matrix

As noted in earlier sections, the subgrade soils having low-to-medium plasticity are more susceptible to pump under adverse loading conditions. Indraratna et al. [31] investigated the influence of the addition of kaolin fines content on the critical number of cycles, N_c. The critical number of cycles was defined as the number of cycles where the axial strains began to increase rapidly. At the same CSR = 0.3, N_c increases from 39 to 105 cycles when mere 10% kaolin is added to the original soil (Fig. 14). However, there is a drop in the critical number of cycles as the fines content is increased to 30%. This may be attributed to the increase in the cohesion in the soil matrix due to the addition of kaolin fines. Thus, the inclusion of a reasonable amount of cohesive fines can enhance the resistance of subgrade to fluidisation and consequent mud pumping under rail tracks when subjected to unfavourable CSR generated by high axle loads (freight trains) [31].

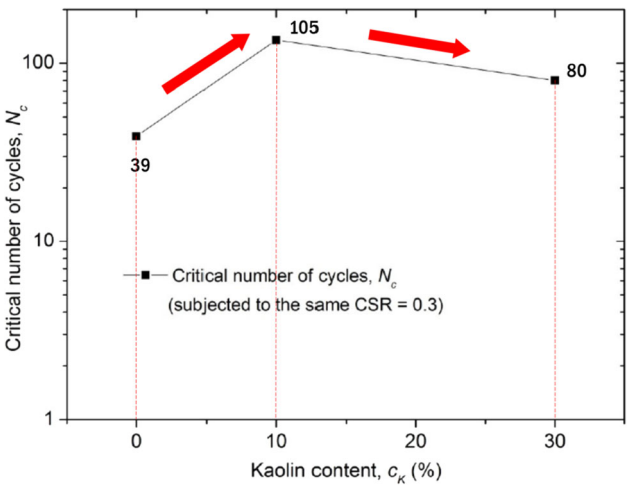

Fig. 14 Influence of cohesive fines inclusion on the critical number of cycles (modified after Indraratna et al. [31])

The Effect of Geosynthetics in Reducing the Risk of Subgrade Fluidisation Potential

Materials and Test Program

Arivalagan et al. [50] performed cyclic tests on three different geotextiles (Tests G1, G2, and G3) to assess the efficacy in preventing particle migration and alleviating subgrade fluidisation potential. The geotextile G1 had a filter membrane in between nonwoven geotextile layers and a filter aperture opening size (O_{95}) of less than 1 µm. The opening size (O_{95}) of G2 and G3 was 60 and 75 µm, respectively [51]. The maximum tensile strength of geotextiles G1, G2, and G3 [52] was 50, 52.5, and 30 kN/m, respectively. The maximum CBR puncture resistance of G1, G2, and G3 was 10 kN, 9 kN. and 5 kN, respectively, as follows EN ISO 12236 [53].

The filtration apparatus developed by Israr and Indraratna [54] was modified to measure the rate of change in excess pore pressure (EPP), time-dependent excess pore pressure gradient (EPPG), and axial strain development under cyclic loading conditions. The modified large-scale dynamic filtration apparatus was used to carry out a series of laboratory experiments by simulating three different drainage conditions, namely: (1) undrained (Test T1), (2) free drainage (Test T2), and (3) partially drained with geosynthetic inclusions. Figure 15 shows the schematic illustration of the key components of the apparatus. Four miniature pressure transducers (MPs) were installed at 20, 40, 80, and 120 mm from the top ballast/subgrade interface. Further, six body transducers (Ps) were installed at 25, 55, 85, 115, 145, and 175 mm from the ballast/subgrade interface on opposite faces of polycarbonate cell to capture the temporal variations in EPPG. A 35-mm-thick layer of fresh ballast layer was placed on the top of the geotextile to simulate the ballast/geotextile interface.

The laboratory tests comprised of five test procedures, including (1) compaction, (2) saturation, (3) consolidation, (4) interface preparation, and (5) loading application. During the compaction, the target bulk density of 1600 kg/m^3 (95% of relative compaction) and moisture content of 17% were attained by compacting the soil under nonlinear undercompaction method. The saturation of the prepared soil specimen was continuously monitored by three amplitude domain reflectometry (ADR) probes at 45, 100, and 155 mm from the ballast/subgrade interface prior to the consolidation. The geotextile was placed below the ballast layer, as shown in Fig. 15.

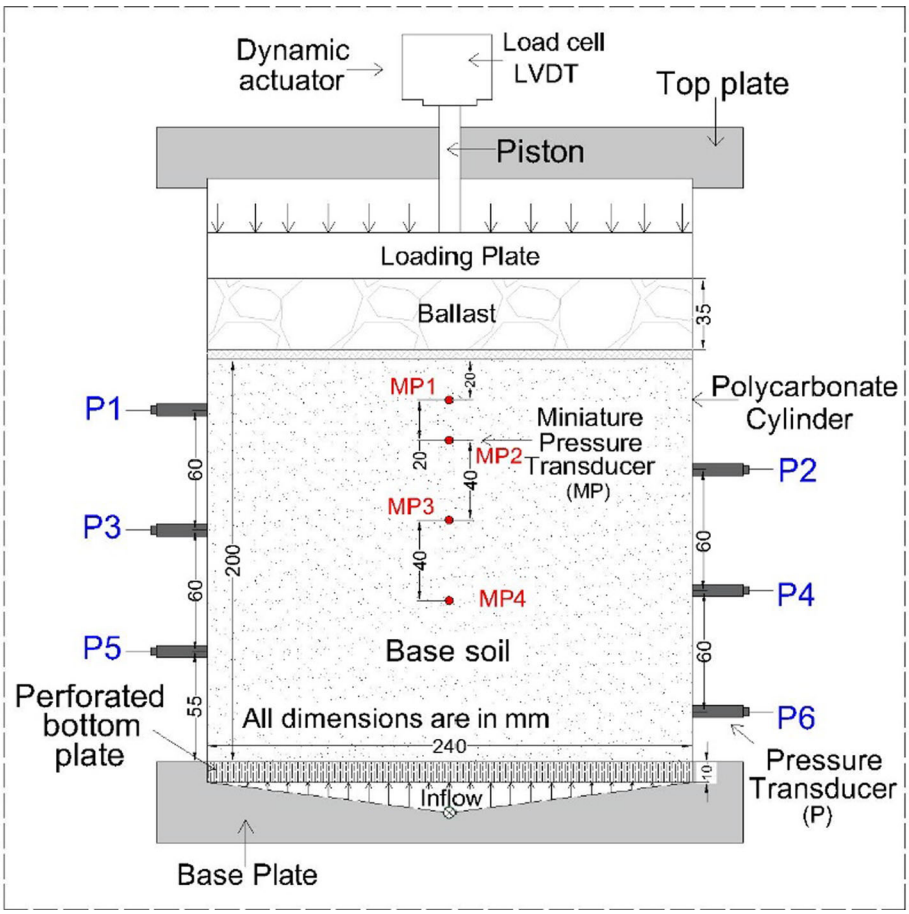

Fig. 15 Schematic cross section of the experimental set-up

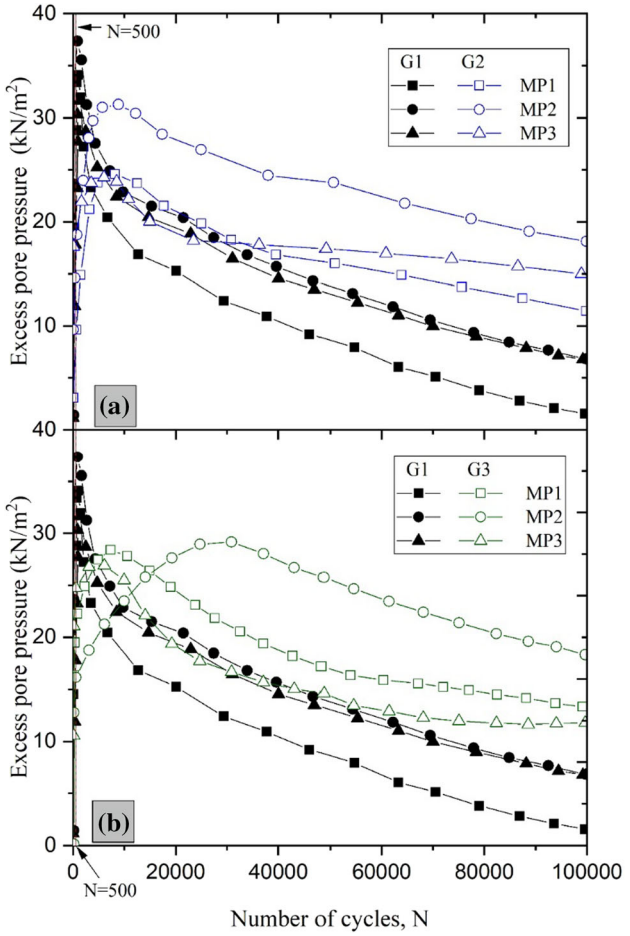

Fig. 16 Excess pore water pressures **a** Tests G1 and G2 **b** Tests G1 and G3 (modified after Arivalagan et al. [50])

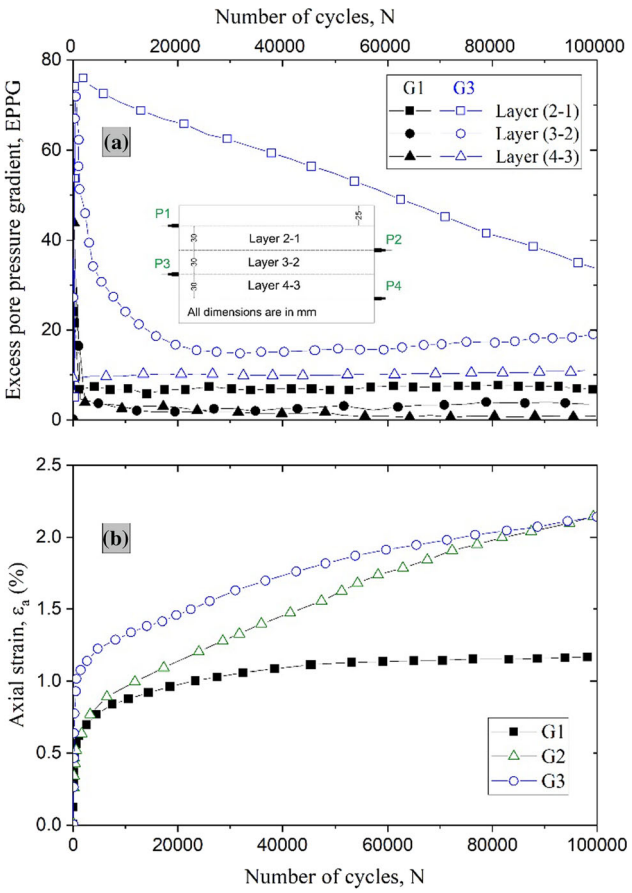

Fig. 17 **a** Excess pore pressure gradients for Tests G1 and G3 and **b** axial strain for Tests G1, G2, and G3 (modified after Arivalagan et al. [50])

Performance of Different Geotextiles under Cyclic Loading

The deviatoric stress of 40 kPa at a frequency of 5 Hz was applied for 100,000 cycles to assess the effectiveness of different geotextiles (G1, G2, and G3). As shown in Fig. 16 geotextile G1 develops a higher EPP (more than 30 kPa) in the first 500 cycles, and it dissipates the EPP to less than 10 kPa at the end of each test. The miniature pressure transducers measured lower than 22 kPa after 10,000 cycles, and G1 could alleviate EPPs with the increase in number of cycles. Unlike other geotextiles (G2, G3), G1 dissipates the EPP by more than 85 and 60% after 100,000 cycles at 20 and 40 mm below the interface, respectively. The rate of dissipation in EPP for G2 and G3 is very low compared to G1, near the interface and the middle region of soil specimen. The larger pore openings in G2 and G3 led to particle migration through the pore openings and became clogged with fines particles, diminishing drainage capacity under cyclic loading conditions.

The EPP measured at different locations by body transducers was used to calculate the excess pore pressure gradient (EPPG). It is defined as the ratio between the change in the excess pore water pressure head and the corresponding distance between two specified locations. The non-uniform development in EPPG (Fig. 17a) generates high upward hydrodynamic force sufficient to dislocate the fines and pump them upwards. The critical layers in middle/deeper subgrade soil were also captured by determining the EPPG at different depths. Figure 17a shows that the EPPG developed in G1 is significantly lower than G3. The EPPGs developed in Layers (2–1) and (3–2) are higher than 70 at 1000 cycles in Test G3 and thus highlighting the potential for particle migration under adverse hydraulic conditions. However, the generation of EPPGs in critical layers (i.e. Layer (3–2) and Layer (2–1)) for Test G1 reduces below ten after 1000 cycles.

A continual increase in axial strain was observed in G2 and G3 due to the pore water pressure dissipation and subsequent particle migration through the geotextiles. Figure 17b shows that the residual axial strain remains below 1.5% for G1, while G2 and G3 show the increasing trend up to 100,000 cycles ($\varepsilon_a < 2.1\%$). The extent of fines trapped in the pore openings in G1, G2, and G3 is 5.92,

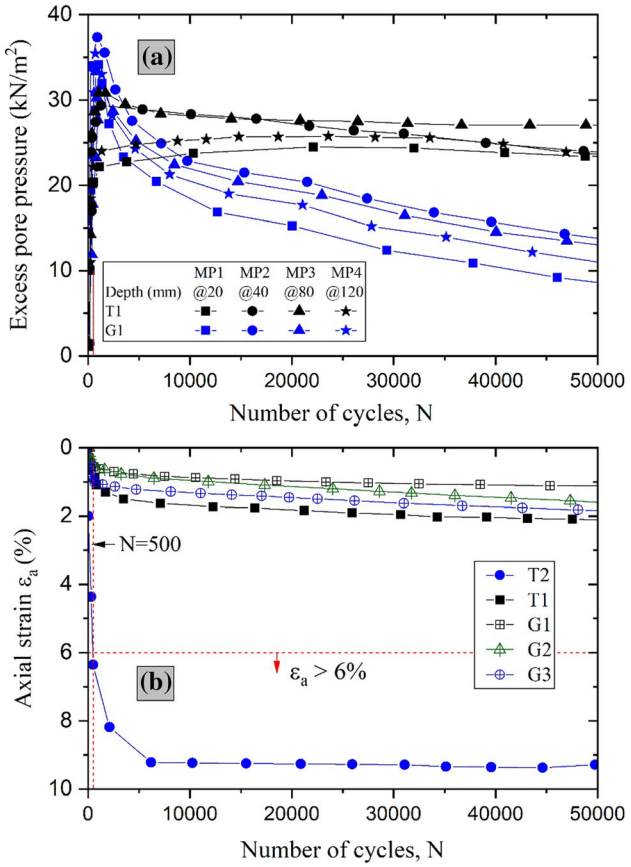

Fig. 18 **a** Excess pore pressures for Tests T1 and G1 **b** axial strain (modified after Arivalagan et al. [50])

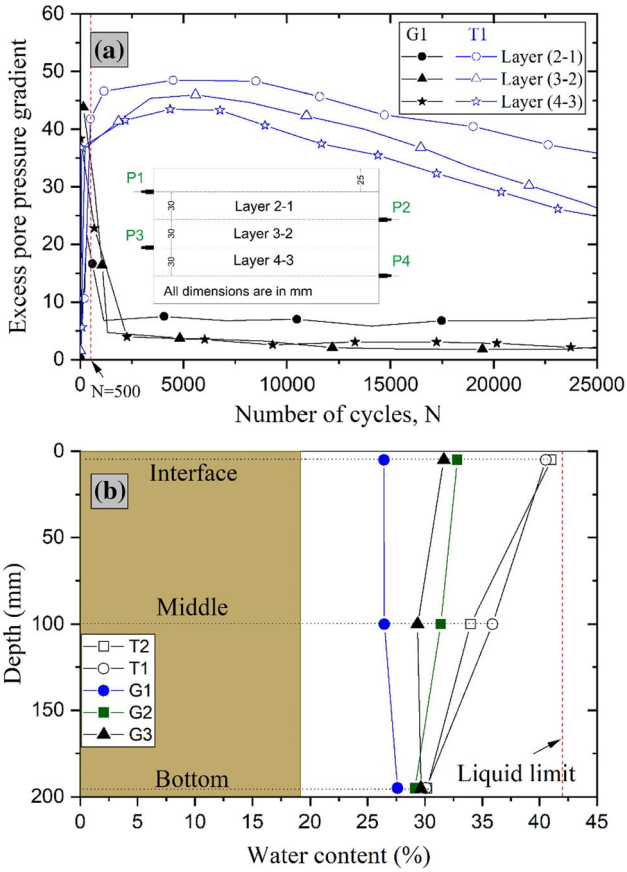

Fig. 19 **a** Excess pore pressure gradients for Tests T1 and G1 and **b** water contents after N = 100,000 cycles (modified after Arivalagan et al. [50])

8.12, and 9.16 g, respectively, and the geotextile area is 4.15×10^{-5} m^2. The larger pore openings in G2 and G3 led to particle migration and more clogging with fines compared to G1. The test results show that G1 effectively reduces EPP accumulation and prevents particle migration under cyclic loading conditions compared to G2 and G3.

Effectiveness of Geotextiles in Reducing the Risk of Subgrade Fluidisation

The undrained (Test T1) and free drainage (Test T2) tests were carried out where an impermeable layer and a layer of ballast were directly placed over the subgrade specimen, respectively. The experiments were also subjected to 40 kPa deviatoric stress at 5 Hz frequency. As shown in Fig. 18a, the EPPs developed at the middle layers (MP2 and MP3) and lower subgrade soils (MP4) were significantly high for Test T1. This implies that the middle layer or a shallow part of subgrade soil is vulnerable to subgrade fluidisation under undrained conditions. However, geotextile G1 can successfully prevent the critical development in EPP, and there is a 52% reduction in EPP observed at MP3 (@100 mm) after 50,000 cycles, as shown in Fig. 18a. The pore development at MP1 (@20 mm from the interface) is further reduced by 64% at 50,000 cycles using G1. The subgrade near the interface becomes slurry in Test T1 and T2 after 500 cycles, where G1 prevents the formation of an 'interlayer' by providing additional confinement at the interface and the onset of subgrade fluidisation. The test results imply that higher EPP without continual dissipation can cause particle separation and associated subgrade fluidisation. However, the rapid EPP developed in middle or lower regions can be alleviated using geotextiles (G1) under adverse hydraulic conditions.

Figure 18b shows that the maximum axial strain developed in Test T2 reaches 6% in just 500 cycles. Similar observations were reported by Indraratna et al. [29], discussing the effect of increased axial strain during the occurrence of subgrade fluidisation. The development of axial strain is controlled due to the inclusion of geotextiles at the interface, and it is less than 1% even after 50,000 cycles. Figure 19a shows the EPPGs developed in Tests T1 shoots above 40 at 500 cycles, and thereafter remained constant until 15,000 cycles. However, G1 significantly reduces the EPPG at the top three layers of

subgrade soil within 1000 cycles, and the EPPGs in Layers (2–1) and (3–2) show 81% and 92% reduction at 25,000 cycles.

Figure 19b shows the efficiency of different geotextiles curtailing the water content of subgrade soil. The water content for undrained and free drainage tests is close to the liquid limit at the top surface of the subgrade and induces subgrade fluidisation as finer particles continuously accumulate under repeated loading conditions. Moreover, G1 helps in reducing the water content, unlike undrained (T1) and free drainage (T2) tests and prevents the potential for softening of the top surface (fluidisation) near the ballast/subgrade interface.

Performance of Geotextiles under Higher Cyclic Stress

The effectiveness of geotextile (G1) must be examined under different axle loads and the speed of the heavy haul trains. Therefore, varying magnitudes of deviatoric stress (σ_{max}) of 70 kPa (Test D70), 85 kPa (Test D85), and 100 kPa (Test D100) were used to simulate the axle load of heavy haul trains. The geotextile G1 was used for this study, and its effectiveness in preventing subgrade fluidisation is discussed in the following sections.

As predicted, expeditious development in EPP was observed when increased the cyclic deviatoric stress was up to 100 kPa. As shown in Fig. 20a, the geotextile G1 was less effective in the middle to the lower region (i.e. critical layers) in Test D100. The miniature pressure transducers (MP2, MP3, and MP4) readings were above 40 kPa and 16 kPa in Tests D100 and D85 until the test ended (80,000 cycles). The increasing trend in axial strain was reported in the past studies [29, 31] when the subgrade soil was subjected to a higher cyclic stress ratio (CSR). The continual increase in axial strain (Test D100) reaches 5% at about 75,000 cycles, as shown in Fig. 20b. In contrast, the axial strain for D70 was less than 1.5%, and it was 2.2% after 80,000 cycles in Test D85.

Figure 21a shows that the maximum EPPG of 120 and 225 developed in less than 1000 cycles in Layers (2–1) and (3–2), respectively, during Tests D85 and D100. However, the EPPGs of the top and middle layers (i.e., Layers (2–1), (3–2) and (4–3)) dropped to 10 immediately after 1000 cycles and remained constant in Test D70. The rate of dissipation in EPPG after 1000 cycles in the critical layers (Layers (3–2) and (4–3)) of soil is minimal at higher cyclic stress levels when compared to lower cyclic deviatoric stress. The water contents of the top and middle layers were significantly reduced due to the inclusion of G1 under lower cyclic stress. There is nearly 5% increase in the water content at the subgrade surface in Test D100, as shown in Fig. 21b. Severe clogging and migrated fine particles were observed at the interface in Tests D100

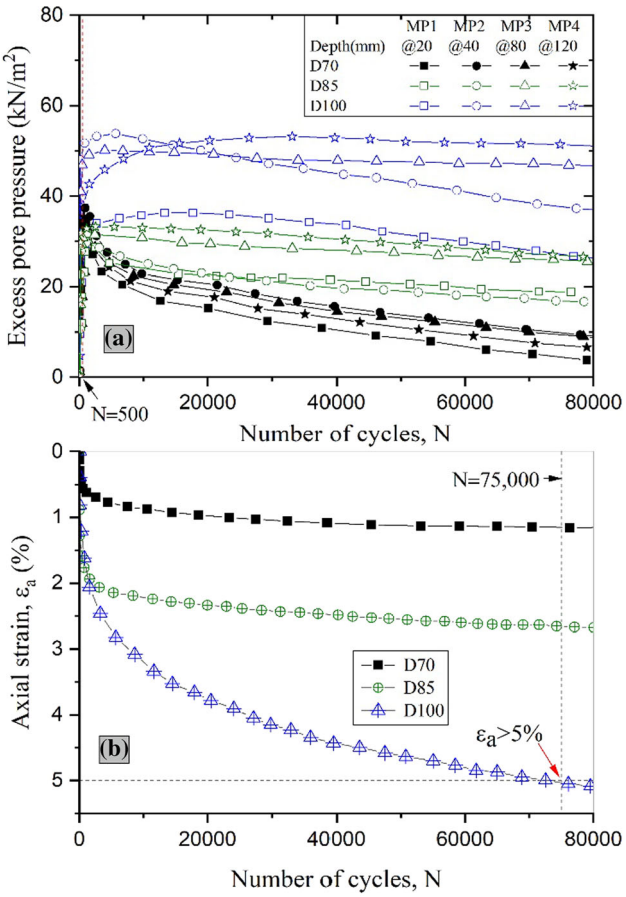

Fig. 20 **a** Excess pore pressures and **b** axial strains under different deviatoric cyclic stress (modified after Arivalagan et al. [50])

compared to Tests D70 and D85. This indicates that G1 was less effective in preventing the abrupt change in water content and subsequent fine particle migration from the middle layers with increased cycles under σ_{max} of 100 kPa. Indeed, the potential for fines migration becomes prominent with increased cyclic stress, and the associated mud pumping can be trigged under repeated loading conditions.

Conclusions

The salient findings from this research are summarised as follows:

- Subgrade mud pumping is commonly observed in ballasted rail tracks. Through an extensive survey of the literature and the ongoing efforts involving various site investigations along the eastern coast of New South Wales, it can be concluded that subgrade soils with low-to-medium plasticity are prone to mud pumping under the current axle loads and speeds of freight trains.
- Undrained cyclic response of the soil prone to mud pumping revealed that it is the sudden rise of axial

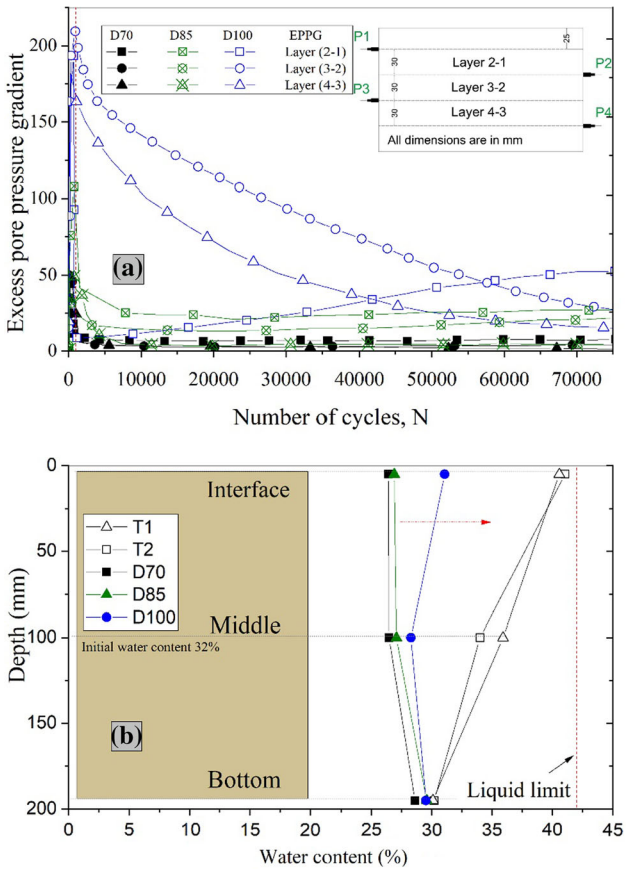

Fig. 21 **a** Excess pore pressure gradients and **b** water contents after $N = 100{,}000$ cycles (Tests D70, D85, and D100) (modified after Arivalagan et al. [50])

strains accompanied by the high cyclic excess pore water pressure that causes the upward migration of finer fraction of the soil. The top portion of the fluidised specimens turned to a liquid-like state with the liquidity index near unity and the specimen stiffness dropped rapidly.

- The migration of fines along with the moisture redistribution is an intrinsic phenomenon during soil fluidisation, and it was addressed by carrying out the discrete element method (DEM) coupled with the computational fluid dynamics (CFD). At higher hydraulic gradients, there was a clear loss of contact network between the soil particles causing upward migration.
- Geosynthetic inclusions such as geotextile (G1) are effective in dissipating the cyclic excess pore water pressure, reducing the overall deformation, and thereby, prevent fine particles migration under cyclic loading conditions. The potential for fines migration becomes significant with increased cyclic stresses, and this can be attributed to the higher hydraulic gradients.

Acknowledgements The authors would like to acknowledge the Australian Research Council (ARC) for supporting this research through the ARC Linkage Project (LP160101254), the ARC Industrial Transformation Training Centre for Advanced Technologies in Rail Track Infrastructure (ITTC-Rail) and the Transport Research Centre (TRC) at the University of Technology Sydney. The financial and technical support from Australasian Centre For Rail Innovation (ACRI), Metro Train Melbourne (MTM), Transport for NSW, Sydney Trains, Global Synthetics, Coffey, SMEC-Australia, and ARTC (Australian Rail Track Corporation) is acknowledged. The efforts of past and current doctoral students Dr Ni Jing, Dr Aruni Abeywickrama, Dr Warantorn Korkitsuntornsan, and Minh Hoang Truong that have contributed to the contents of this keynote paper are also greatly appreciated. A significant portion of the contents included in this Keynote paper has been published earlier in scholarly journals by Professor Indraratna and co-workers and reproduced herein with kind permission obtained from original sources such as ASCE-JGGE, Canadian Geotechnical Journal, Transportation Geotechnics, Computers, and Geotechnics among others.

Funding Open Access funding enabled and organized by CAUL and its Member Institutions.

Declarations

Conflict of interest The authors declare that they have no conflict of interest.

References

1. Indraratna B, Salim W (2005) Mechanics of ballasted rail tracks: a geotechnical perspective. CRC Press, Boca Raton
2. Selig ET, Waters JM (1994) Track geotechnology and substructure management. Thomas Telford, London
3. Pons JJ, Villalba Sanchis I, Insa Franco R, Yepes V (2020) Life cycle assessment of a railway tracks substructures: comparison of ballast and ballastless rail tracks. Environ Impact Assess Rev 85:106444
4. Koohmishi M (2019) Drainage potential of degraded railway ballast considering initial gradation and intrusion of external fine materials. Soils Found 59(6):2265–2278
5. Tennakoon N, Indraratna B, Rujikiatkamjorn C, Nimbalkar S, Neville T (2012) The role of ballast-fouling characteristics on the drainage capacity of rail substructure. Geotech Test J 35(4):629–640
6. Indraratna B, Nimbalkar SS, Tennakoon N (2010) The behaviour of ballasted track foundations: track drainage and geosynthetic reinforcement. American Society of Civil Engineers, Reston

7. Ngamkhanong C, Feng B, Tutumluer E, Hashash YMA, Kaewunruen S (2021) Evaluation of lateral stability of railway tracks due to ballast degradation. Constr Build Mater 278:122342
8. Li X, Vanapalli SK (2021) Simulation of progressive shear failure in railway foundation. Transp Geotech 29:100550
9. Nguyen TT, Indraratna B (2021) Rail track degradation under mud pumping evaluated through site and laboratory investigations. Int J Rail Transp 10(1):44–71
10. Li D (2018) 25 years of heavy axle load railway subgrade research at the Facility for Accelerated Service Testing (FAST). Transp Geotech 17:51–60
11. Sánchez M, Wang D, Briaud J-L, Douglas C (2014) Typical geomechanical problems associated with railroads on shrink-swell soils. Transp Geotech 1(4):257–274
12. Duong TV, Cui Y-J, Tang AM, Dupla J-C, Canou J, Calon N, Robinet A (2014) Investigating the mud pumping and interlayer creation phenomena in railway sub-structure. Eng Geol 171:45–58
13. Li D, Selig ET (1998) Method for railroad track foundation design I: development. J Geotech Geoenviron Eng 124(4):316–322
14. Singh M, Indraratna B, Nguyen TT (2021) Experimental insights into the stiffness degradation of subgrade soils prone to mud pumping. Transp Geotech 27:100490
15. Hudson A, Watson G, Le Pen L, Powrie W (2016) Remediation of mud pumping on a ballasted railway track. Proc Eng 143:1043–1050
16. Huang J, Qian S, Liu T, Wang W (2019) Behavior and control of the ballastless track-subgrade vibration induced by high-speed trains moving on the subgrade bed with mud pumping. Shock Vib 2019:1–14
17. Nguyen TT, Indraratna B, Kelly R, Phan NM, Haryono F (2019) Mud pumping under railtracks: mechanisms, assessments and solutions. Aust Geomech J 54(4):59–80
18. Hayashi S, Shahu JT (2000) Mud pumping problem in tunnels on erosive soil deposits. Géotechnique 50(4):393–408
19. Ayres DJ (1986) Geotextiles or geomembranes in track? British railways' experience. Geotext Geomembr 3(2–3):129–142
20. Duong TV, Tang AM, Cui Y-J, Trinh VN, Dupla J-C, Calon N, Canou J, Robinet A (2013) Effects of fines and water contents on the mechanical behavior of interlayer soil in ancient railway substructure. Soils Found 53(6):868–878
21. Trani LDO, Indraratna B (2010) Assessment of subballast filtration under cyclic loading. J Geotech Geoenviron Eng 136(11):1519–1528
22. Alobaidi I (1996) The development of pore water pressure at the subgrade-subbase interface of a highway pavement and its effect on pumping of fines. Geotext Geomembr 14(2):111–135
23. Kuo C (2021) Ground-penetrating radar to investigate mud pumping distribution along a railway line. Constr Build Mater 290:123104
24. Takatoshi I (1997) Measure for the stabilization of railway earth structure. Jpn Railw Tech Serv, Tokyo, Japan
25. Li D, Selig E (1995) Evaluation of railway subgrade problems. Transp Res Rec 1489:17
26. De Bold R, Connolly DP, Patience S, Lim M, Forde MC (2021) Using impulse response testing to examine ballast fouling of a railway trackbed. Constr Build Mater 274:121888
27. Indraratna B, Salim W, Rujikiatkamjorn C (2011) Advanced rail geotechnology-ballasted track. CRC Press, Boca Raton
28. Selig E, DelloRusso V, Laine K (1992) Sources and causes of ballast fouling. Association of American Railroad (AAR), Report No. R-805, Technical Center, Chicago
29. Indraratna B, Singh M, Nguyen TT, Leroueil S, Abeywickrama A, Kelly R, Neville T (2020) Laboratory study on subgrade fluidization under undrained cyclic triaxial loading. Can Geotech J 57(11):1767–1779
30. Chawla S, Shahu JT (2016) Reinforcement and mud-pumping benefits of geosynthetics in railway tracks: model tests. Geotext Geomembr 44:366–380
31. Indraratna B, Korkitsuntornsan W, Nguyen TT (2020) Influence of Kaolin content on the cyclic loading response of railway subgrade. Transp Geotech 22:100319
32. Voottipruex P, Roongthanee J (2003) Prevention of mud pumping in railway embankment. A case study from Baeng Pra-Pitsanuloke, Thailand. J KMITB 13(1):20–25
33. Indraratna B, Attya A, Rujikiatkamjorn C (2009) Experimental investigation on effectiveness of a vertical drain under cyclic loads. J Geotech Geoenviron Eng 135(6):835–839
34. Indraratna B, Rujikiatkamjorn C, Ewers B, Adams M (2010) Class A prediction of the behavior of soft estuarine soil foundation stabilized by short vertical drains beneath a rail track. J Geotech Geoenviron Eng 136(5):686–696
35. Nguyen TT, Indraratna B, Carter J (2018) Laboratory investigation into biodegradation of jute drains with implications for field behavior. J Geotech Geoenviron Eng 144(6):04018026
36. Nguyen TT, Indraratna B (2019) Micro-CT scanning to examine soil clogging behavior of natural fiber drains. J Geotech Geoenviron Eng 145(9):04019037
37. Trinh VN, Tang AM, Cui Y-J, Dupla J-C, Canou J, Calon N, Lambert L, Robinet A, Schoen O (2012) Mechanical characterisation of the fouled ballast in ancient railway track substructure by large-scale triaxial tests. Soil Found Jpn Geotech Soc 52(3):511–523
38. Indraratna B, Tennakoon N, Nimbalkar S, Rujikiatkamjorn C (2013) Behaviour of clay-fouled ballast under drained triaxial testing. Géotechnique 63(5):410–419
39. ASTM:D2487–17, Standard Practice for Classification of Soils for Engineering Purposes (Unified Soil Classification System) 1. 2017: ASTM International
40. Muramoto K, Nakamura T (2011) Development of the countermeasure against roadbed degradation under ballastless tracks for existing lines. In: 9th World Congress on Railway Research
41. Liu D, He Lin F, Zhu XZ, Liu YS, Rao JY (2013) Study on the remediation of mud-pumping. Appl Mech Mater 275–277:1560–1563
42. Duong TV, Cui Y-J, Tang AM, Dupla J-C, Canou J, Calon N, Robinet A, Chabot B, De Laure E (2014) Physical Model for Studying the Migration of Fine Particles in the Railway Substructure. Geotech Test J 37(5):20130145
43. ASTM:D4767–95 (1995) Standard test method for consolidated undrained triaxial compression test for cohesive soils. ASTM International
44. Zhou J, Gong X (2001) Strain degradation of saturated clay under cyclic loading. Can Geotech J 38(1):208–212
45. Lei H, Li B, Lu H, Ren Q (2016) Dynamic deformation behavior and cyclic degradation of ultrasoft soil under cyclic loading. J Mater Civ Eng 28(11):04016135
46. Indraratna B, Singh M, Nguyen TT (2020) The mechanism and effects of subgrade fluidisation under ballasted railway tracks. Railw Eng Sci 28(2):113–128
47. Nguyen TT, Indraratna B (2020) The energy transformation of internal erosion based on fluid-particle coupling. Comput Geotech 121:103475
48. Nguyen TT, Indraratna B (2020) A coupled CFD-DEM approach to examine the hydraulic critical state of soil under increasing hydraulic gradient. ASCE Int J Geomech 20(9):04020138
49. Fleshman MS, Rice JD (2014) Laboratory modeling of the mechanisms of piping erosion initiation. J Geotech Geoenviron Eng 140(6):04014017

50. Arivalagan J, Rujikiatkamjorn C, Indraratna B, Warwick A (2021) The role of geosynthetics in reducing the fluidisation potential of soft subgrade under cyclic loading. Geotext Geomembr 49:1324
51. ASTM F316–03 (2003) Standard Test Methods for Pore Size Characteristics of Membrane Filters by Bubble Point and Mean Flow Pore Test. 2011, ASTM International, West Conshohocken, PA
52. EN ISO 10319, Geosynthetics–Wide-width tensile test. . 2008, International Organization for Standardization, Geneva, Switzerland
53. EN ISO 12236, Geosynthetics—Static Puncture Test (CBR Test). 2006, European Committee for Standardization, Brussels, Belgium
54. Israr J, Indraratna B (2017) Internal stability of granular filters under static and cyclic loading. J Geotech Geoenviron Eng 143(6):04017012